Chemical Science

ROYAL SOCIETY OF CHEMISTRY

EDGE ARTICLE

View Article Online
View Journal | View Issue

Cite this: *Chem. Sci.*, 2023, **14**, 11359

All publication charges for this article have been paid for by the Royal Society of Chemistry

Received 6th July 2023
Accepted 17th September 2023

DOI: 10.1039/d3sc03465h

rsc.li/chemical-science

Visible light activated energy storage in solid-state Azo-BF_2 switches†

Qianfeng Qiu,‡[a] Qingkai Qi,‡[b] Junichi Usuba,[a] Karina Lee,[a] Ivan Aprahamian *[b] and Grace G. D. Han *[a]

We present here a group of Azo-BF_2 photoswitches that store and release energy in response to visible light irradiation. Unmodified Azo-BF_2 switches have a planar structure with a large π-conjugation system, which hinders *E*–*Z* isomerization when in a compacted state. To address this challenge, we modified the switches with one or two aliphatic groups, which altered the intermolecular interactions and arrangement of the photochromes in the solid state. The derivative with two substituents exhibited a non-planar configuration that provided particularly large conformational freedom, allowing for efficient isomerization in the solid phase. Our discovery highlights the potential of using double aliphatic functionalization as a promising approach to facilitate solid-state switching of large aromatic photoswitches. This finding opens up new possibilities for exploring various photoswitch candidates for molecular solar thermal energy storage applications.

Introduction

Molecular solar thermal (MOST) energy storage compounds, which absorb and store photon energy through photoisomerization and release the energy as heat when triggered to undergo the reverse isomerization, have emerged as a promising solution for harnessing and storing wasted solar energy. Various photoswitches, including fulvalene diruthenium complexes,[1–4] norbornadienes,[5–8] dihydroazulenes,[9–12] azo(hetero)arenes,[13–17] and hydrazones,[18] have been investigated and reported for successful MOST energy storage, as a result of the reversible isomerization of the switches and considerable energy difference between the thermodynamically stable isomer and its metastable photoisomer. Considerable efforts have been dedicated to validating the functional substituents of the aforementioned photoswitches to enhance their optical and thermal properties[19–23] *e.g.*, quantum yields of switching, photostationary state (PSS) ratios of isomers, absorption wavelengths, and thermal stability of metastable-state isomers. The characterization of the parameters is primarily performed in dilute solutions, while the translation of such properties in condensed phases, particularly in the solid state, is critical for developing MOST systems with large gravimetric and volumetric energy densities.[24] However, the solid-state isomerization of photoswitches is often unfavourable because of the significantly reduced conformational freedom of molecules in the condensed phases, especially for transformations that require a large structural and volumetric change of isomers.[25] In addition, most of the established MOST compounds primarily absorb light in the UV range to activate the thermodynamically stable state,[16] which limits the use of the solar spectrum that contains only about 5% UV photons.[26]

In pursuit of visible and/or near IR activated photoswitches, a series of Azo-BF_2 complexes were developed,[27–30] which exhibit red-shifted π_{nb}–π* and blue-shifted n–π* transitions caused by the coordination of the azo moiety with the Lewis acid (BF_2).[27] The control over the absorption wavelengths, photoisomerization quantum yields, PSS ratios, and thermal half-lives of the *Z* isomer was demonstrated through the modular design of Azo-BF_2 compounds bearing various functional groups.[28] Because of the limited examples of MOST compounds that can be activated by long visible or near IR light, the Azo-BF_2 design presents a unique opportunity to harness the longer end of the solar spectrum, complementary to the conventional MOST compounds that absorb UV or short visible light.[16] However, the evaluation of Azo-BF_2 for MOST applications has not been explored, because the planarity of the large photochromic core induces significant π interactions that reduce the conformational freedom of the photoswitches in condensed phases. Such interactions were preliminarily investigated in concentrated solutions of Azo-BF_2 that resulted in aggregation and impacted the thermal reversion half-life of the *Z* isomers.[31]

[a]*Department of Chemistry, Brandeis University, 415 South Street, Waltham, MA 02453, USA. E-mail: gracehan@brandeis.edu*

[b]*Department of Chemistry, Dartmouth College, Hanover, NH 03755, USA. E-mail: ivan.aprahamian@dartmouth.edu*

† Electronic supplementary information (ESI) available: Methods, synthesis, UV-Vis spectra, quantum yield, TGA, DSC, kinetic analysis, film studies, DFT results, X-ray diffraction. CCDC 2257907–2257910. For ESI and crystallographic data in CIF or other electronic format see DOI: https://doi.org/10.1039/d3sc03465h

‡ Equal contributions.

Herein, we report the design principle of Azo-BF_2 derivatives that enables reversible photoswitching in the solid state, exclusively triggered by visible light. We present the first demonstration of MOST energy storage in Azo-BF_2 compounds, facilitated by the introduction of aliphatic substituents that display out-of-plane distortion and reduce π interactions among the Azo-BF_2 cores. Unlike previous reports that demonstrated solid–liquid phase transitions of azobenzenes or arylazopyrazoles that are functionalized with an aliphatic group,[14,15,32–34] the Azo-BF_2 derivatives exhibit unique solid-state transitions and solar energy storage.

Results and discussion

Four mono-substituted (compounds **1–4**) and one di-substituted (compound **5**) derivatives of Azo-BF_2 (Fig. 1a) were synthesized in 35–60% yield by reacting their hydrazone precursors with boron trifluoride diethyl etherate in the presence of *N*,*N*-diisopropylethylamine.[27] The Azo-BF_2 switches and all their precursors were fully characterized using NMR spectroscopy and mass spectrometry. The UV-Vis absorption spectra of all the Azo-BF_2 compounds were comparable (Fig. S1†), exhibiting a broad peak around 590 nm corresponding to the π_{nb}–π* transition of the *E* isomer and blue-shifted absorption around 520 nm for the *Z* counterpart (Fig. 1b). Both *E* and *Z* isomers show around 65 nm and 45 nm bathochromic shifts, respectively, compared to the absorption peaks of the pristine Azo-BF_2 switch.[27] These significant absorption shifts are attributed to the *para*-functionalization of the alkyloxy groups, which extends the π conjugation in the system and results in a smaller HOMO–LUMO energy gap. The PSS ratios of the *E*/*Z* isomers of all the Azo-BF_2 compounds under 625 and 470 nm irradiation (PSS_{625} and PSS_{470}, respectively) were evaluated in dichloromethane (DCM): PSS_{625} = 90–97% *Z* and PSS_{470} = 48–59% *E* (Fig. S2–S6†). All PSS ratios and quantum yields of switching are summarized in Fig. S7–S16 and Table S1.† The relatively low PSS_{470} is mainly because of the *E*/*Z* spectral overlap. The thermal half-lives of the five *Z* isomers were also examined in DCM at 20 °C and found to be between 7 and 69 min (Fig. S17 and Table S2†). In the MOST context, 625 nm irradiation induces *E* → *Z* conversion, which stores the isomerization energy (ΔH_{iso}) in the chemical bonds of the metastable *Z* isomer (Fig. 1a), which is then released as heat upon *Z* → *E* back-isomerization using 470 nm irradiation. The alkyloxy substituents on the Azo-BF_2 core, marked as R_1 and R_2, were varied to fine-tune the intermolecular interactions of the compounds in the condensed phase, allowing us to study the impact of such interactions on the molecular packing and photo-switching yields in the solid state.

We examined the thermal stability of all the Azo-BF_2 derivatives using thermogravimetric analysis (TGA) (Fig. S18†), and the phase of their *E* and *Z* isomers by differential scanning calorimetry (DSC) (Fig. 2 and S19†). The DSC plots of compounds **2** and **5** are shown in Fig. 2 as an example. As a result of the extended planar structure of the Azo-BF_2 core, all the *E* isomers display crystalline phases with high melting points (T_m) as listed in Table 1. Compound **1**-*E*, functionalized with a short ethoxy group, exhibits the highest T_m (>164 °C) among all the compounds, which is accompanied by thermal decomposition. Compounds **3**-*E* and **4**-*E*, featuring extended alkoxyl groups, exhibit notably lower melting points at 124 °C. This observation contradicts the typical trend observed in paraffins, where longer chains with enhanced London dispersion forces tend to result in higher melting points.[35,36] This unusual phenomenon bears resemblance to previous reports involving some alkyl-functionalized azo(hereto)arene photoswitches,[14,33,37–39] where the introduction of lengthy alkyl chains also resulted in a significant reduction in melting points.

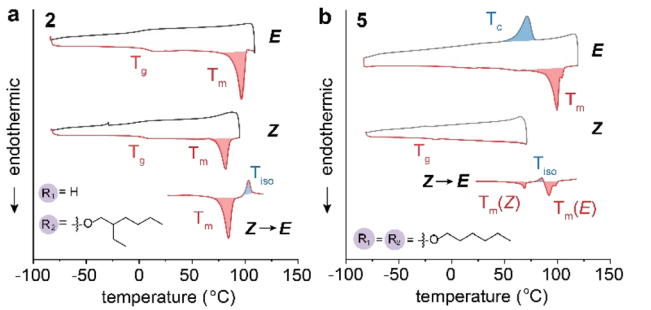

Fig. 2 DSC plots of compounds (a) **2** and (b) **5** as *E* and *Z* isomers measured during the first heating and cooling cycles. Further heating of the *Z* isomers results in *Z* → *E* isomerization and heat release (exotherm highlighted in blue).

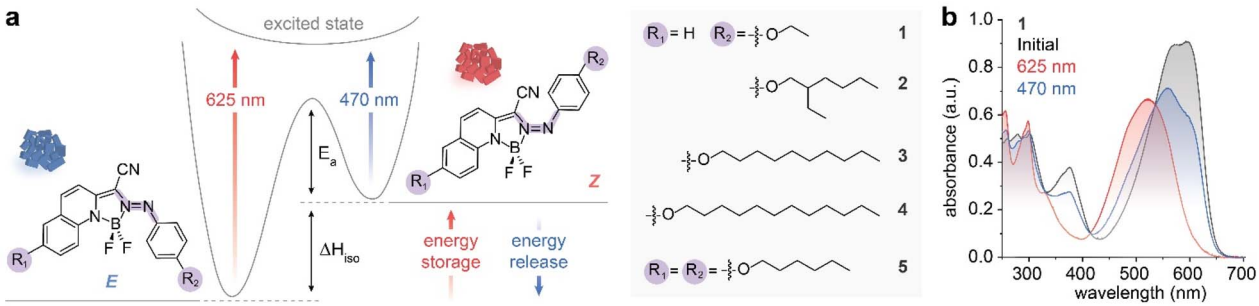

Fig. 1 (a) Chemical structures of Azo-BF_2 derivatives and the diagram of visible-light-triggered photon energy storage and release processes in the solid state. (b) UV-Vis spectral changes upon the photo-irradiation of compound **1** in dichloromethane (2×10^{-5} M).

Table 1 Thermal properties of the *E* and *Z* isomers of compounds **1–5**[a]

	E		*Z*		*Z* → *E*		
	T_m (°C)	ΔH_m (kJ mol^{-1})	T_m (°C)	ΔH_m (kJ mol^{-1})	T_{iso} (°C)	ΔH_{iso} (kJ mol^{-1})	$\tau_{1/2}$ (min)
1	>164	—	>107	—	117	7	69
2	97	21	82	12	104	4	50
3	124	54	66	1	90	20	11
4	124	70	100	17	101	22	36
5	100	19	70	3	87	3	7

[a] T_m: melting point, ΔH_m: melting enthalpy, T_{iso}: isomerization temperature, ΔH_{iso}: isomerization enthalpy, $\tau_{1/2}$: thermal half-life at room temperature, —: unable to measure.

This observation in the case of **3**-*E* and **4**-*E* can be attributed to the weakening of π interactions among the aromatic photoswitch cores (*vide infra*). Compound **2**-*E* with a branched 2-ethylhexyloxy group was designed to lower the T_m to 97 °C by further reducing the π interactions (Fig. 2a), which is a commonly applied strategy in forming a liquid-phase MOST compound.[15,40] Nevertheless, strong π stacking of the photochroms results in the formation of a crystalline solid. Moreover, compounds **1–4** show high melting points (>66 °C) for their *Z* isomers as well, because of the planarity of the *Z* configurations. Most importantly, none of these derivatives underwent *E* → *Z* photo-isomerization in the solid state, as a consequence of the strong π interactions.

Therefore, the substitution of both ends of the Azo-BF_2 with alkyloxy groups was explored as a new strategy to further reduce the intermolecular interactions in both the *E* and *Z* isomers. As shown in Fig. 2b, compound **5**-*E* displays a low T_m of 100 °C, similar to that of compound **2**-*E* (96 °C), and a T_m of **5**-*Z* at 70 °C that is comparable to the lowest T_m of **3**-*Z* (66 °C). Surprisingly, despite the crystallinity of both the *E* and *Z* phases, compound **5** undergoes facile and reversible *E*/*Z* isomerization in the solid state (*vide infra*). All the thermal parameters of compounds **1–5** measured by DSC are summarized in Table 1. In general, the *Z* isomers exhibit 15–58 °C lower T_m values than the corresponding *E* isomers, and the crystal packing differences between the *E* and *Z* isomers are corroborated and elucidated by the powder X-ray diffraction measurements (Fig. S20†).

The measurement of DSC exotherms associated with the *Z* → *E* back-isomerization allows for the evaluation of the density of energy storage (ΔH_{iso}) in each compound. For example, thermal activation of **2**-*Z* leads to the melting of *Z* at 82 °C, followed by back-isomerization (Fig. 2a). Compound **5**-*Z*, similar to **1**-*Z*, **3**-*Z*, and **4**-*Z*, displays the first melting of *Z*, then *Z* → *E* back-isomerization, subsequent crystallization of *E*, and the melting of the formed *E* crystals (Fig. 2b and S19†). The accurate measurement of ΔH_{iso} is challenging because of the convoluted processes. The values of the exotherm peaks are summarized in Table 1. Overall, the ΔH_{iso} values of Azo-BF_2 derivatives are lower than those of azo(hetero)arenes, indicating that the *Z* isomer is not as strained as in these systems. DFT calculations (Fig. S21 and Tables S3–S10†) corroborate the experimental results, predicting ΔH_{iso} values of 19–25 kJ mol^{-1} (Table S11†), which is significantly lower than the value predicted (62 kJ mol^{-1}) or experimentally measured (49 kJ mol^{-1}) for pristine azobenzene.[41] We also note that excessive heating above 125 °C can lead to the partial (∼20%) thermal decomposition of the Azo-BF_2 derivatives, and subsequent formation of their hydrazone precursors, which can also impact the accuracy of the enthalpy measurements.

As aforementioned, compound **5** undergoes reversible solid-state *E*/*Z* isomerization under 625 and 470 nm irradiation, as opposed to the other compounds that do not isomerize in the solid state. Thin films of compounds **1–5** (0.1–0.75 μm thick) were prepared (Fig. S22–S26†), irradiated with a 625 nm LED for 10 min and a 470 nm LED for 2 min, and evaluated by UV-Vis absorption and NMR spectroscopy. Negligible colour change was observed for compounds **1–4** upon irradiation (Fig. 3a and S27†), and small changes in optical spectra (Fig. 3a and S28†) and *Z* percentage (Fig. S29–S32†) of the films were detected. Notably, compound **4** with the longest alkyloxy substituent rapidly (within a minute) aggregates in the cast film, forming large domains that scatter light and induce substantial changes to the absorption profiles. The aggregated state is not altered by the irradiation, and the absorption profile of compound **4** remains unchanged (Fig. S28†).

Compound **5** also shows aggregation-induced reduction of absorbance in films compared to the initially cast state (Fig. S28†), but the reversible photoswitching of *E*/*Z* in films (average thickness of 0.37 ± 0.17 μm, Fig. S26†) was monitored upon 625 and 470 nm irradiation (Fig. 3b). The optical microscopy images clearly demonstrate the colour changes between blue (PSS_{470} 48% *E*) and red (PSS_{625} 70% *Z*) (Fig. S33†). Compared to the solution state, the PSS ratios obtained in the condensed phase are lower, which is attributed to the incomplete penetration of 470 nm (0.22 μm through *E*) and 625 nm (0.47 μm through *Z*) lights (Fig. S34†) and uneven film thickness. The effect of light penetration was confirmed by the irradiation experiment on thinner films (average thickness of 0.18 ± 0.09 μm), which displayed an improved PSS_{625} of 81% *Z* and similar PSS_{470} of 47% *E* (Fig. S35†). We note that the reduced conformational freedom of the photoswitches in the solid state also contributes to the lower PSS ratios. The switching is repeatable over 10 cycles (Fig. 3c), displaying small variations in absorbance after each cycle, which is intrinsic to solid-state UV-Vis measurement of films with imperfect uniformity. Additionally, 17% of photo-degradation was detected by NMR for the thin films after 10 cycles of irradiation (Fig. S36†), which can also induce small absorbance changes. The thermal half-life of **5**-*Z* at 20 °C

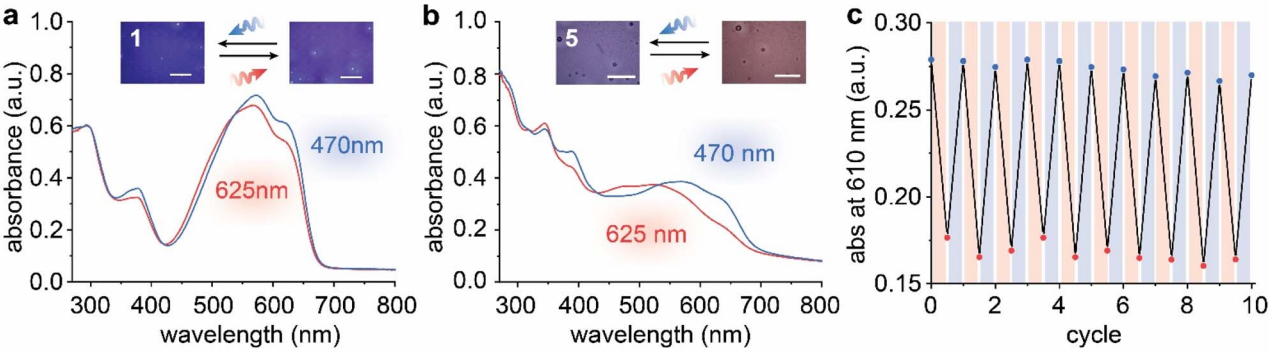

Fig. 3 UV-Vis absorption spectra and optical microscopy images of thin films (a) **1** and (b) **5** upon irradiation at 625 nm (15% **1**-*Z*; 70% **5**-*Z* at PSS) and at 470 nm (17% **1**-*Z*; 48% **5**-*Z* at PSS). Scale bar = 1 mm. (c) Isomerization cycles of thin film **5** upon alternating irradiation at 625 nm for 10 min (red filled area) and at 470 nm for 1 min (blue filled area), monitored by the absorbance changes at 610 nm.

was characterized to be over 4 days (Fig. S37 and Table S12†), significantly extended from that measured in solution (7 min), which indicates the sterically hindered thermal back-isomerization of the compound in films.[31,42]

To elucidate the mechanism behind the unique photo-switchability of compound **5** in films, we performed crystal structure analysis of compounds **1** and **3**–**5** in the *E* isomeric state (Table S13 and Fig. S38–S53†). **2**-*E* did not form high-quality crystals suitable for X-ray diffraction. Fig. 4a shows the twisted head-to-head packing of **1**-*E*, formed by π stacking of Azo-BF_2 cores. Within the structures of **3**-*E* and **4**-*E*, the long alkyloxy chains assume an important role in mediating parallel molecular stacking driven by London dispersion forces. Also, the interaction between the electron-rich phenolic moiety and electron-poor Azo-

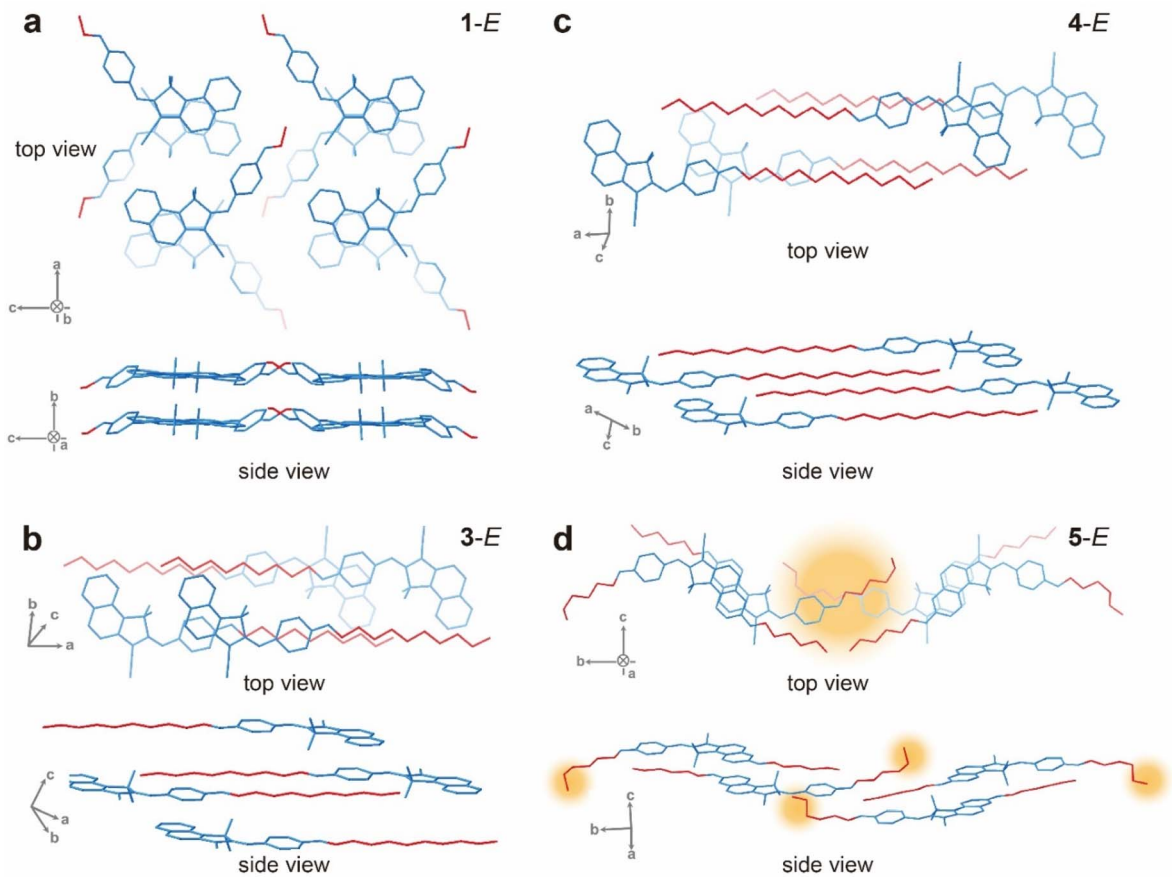

Fig. 4 Crystal structures of (a) **1**-*E*, (b) **3**-*E*, (c) **4**-*E*, and (d) **5**-*E* displayed in two perspectives: top view (top) and side view (bottom). Azo-BF_2 chromophores are coloured in blue, functional groups (R_1 and R_2) in red, and hydrogen atoms are omitted for clarity. Note: high quality crystals of **2**-*E* were not obtained.

BF_2 induces an offset molecular arrangement (Fig. 4b and c). Interestingly, the crystal structure of **5**-*E* does not exhibit any noticeable inter-chain interactions or aligned alkyloxy chains, presumably because of the shorter substituents that do not yield significant London dispersion forces in the offset arrangement. Instead, **5**-*E* displays pronounced π stacking between the neighbouring Azo-BF_2 cores (Fig. 4d), similar to **1**-*E*. The alkyloxy groups show staggered arrangement (top view, yellow highlighted) and out-of-plane distortion in the crystal lattice (side view, yellow highlighted), which clearly differentiates **5**-*E* from the other compounds. This unique packing of compound **5** is hypothesized to reduce the intermolecular interactions in the solid state, which is manifested as low T_m and melting enthalpies of both the *E* and *Z* isomers (Table 1). In addition, the van der Waals space fill models that are obtained based on the crystal structures illustrate the largest fraction of void space (29.5%) in compound **5** compared to the others (23.8–27.5%) (Fig. S41, S45, S49, and S53†). This finding reveals an important strategy for enabling solid-state isomerization of large planar photochromic compounds such as Azo-BF_2 through the introduction of two aliphatic chains into the core structure, which creates a non-linear geometry of the compound that is less prone to compact packing in the solid state. The balance between the π interactions among the aromatic cores and London dispersion[43–47] among the aliphatic chains is critical to decrease the overall intermolecular interactions and increase the conformational freedom needed for isomerization in the solid state.

Conclusions

We developed red light absorbing MOST compounds based on Azo-BF_2 photoswitches and demonstrated that they display reversible photoswitching and energy storage in the solid state. The limited scope of exclusively visible light activated MOST compounds makes this finding unique and valuable for solar energy conversion and storage applications. Through rigorous crystal structure analysis, we established a design principle of double aliphatic functionalization, which reduces the intermolecular interactions and enables the facile solid-state switching of large aromatic photoswitches that are unable to switch otherwise. We believe that this strategy will be widely applicable for various other photoswitches that consist of extended aromatic cores, and which are only investigated in dilute solutions.[48–51] Such investigations will open the way for discovering new MOST compounds having desirable optical and energy storage properties.

Data availability

All experimental data and detailed experimental procedures are available in the published article and ESI.†

Author contributions

Q. Qiu performed optical, thermal, and structural characterization of compounds. Q. Qi synthesized compounds and provided crystal structures. J. U. conducted DFT calculations and analysed crystal structures. K. L. performed TGA and supplementary UV-Vis absorption spectroscopy. G. G. D. H. and I. A. designed, conceived, and supervised the project.

Conflicts of interest

There are no conflicts to declare.

Acknowledgements

This material is based upon work supported by the Air Force Office of Scientific Research under Award Number FA9550-22-1-0254. G. G. D. H. acknowledges the NSF CAREER award (DMR-2142887) and Alfred P. Sloan Foundation (FG-2022-18328). K. L. was supported by Brandeis MRSEC SMURF program (DMR-2011846). I. A. acknowledges the generous support from NSF DMR (2104464).

Notes and references

1 Y. Kanai, V. Srinivasan, S. K. Meier, K. P. C. Vollhardt and J. C. Grossman, *Angew. Chem., Int. Ed.*, 2010, **49**, 8926–8929.
2 K. Börjesson, A. Lennartson and K. Moth-Poulsen, *J. Fluorine Chem.*, 2014, **161**, 24–28.
3 K. Moth-Poulsen, D. Ćoso, K. Börjesson, N. Vinokurov, S. K. Meier, A. Majumdar, K. P. C. Vollhardt and R. A. Segalman, *Energy Environ. Sci.*, 2012, **5**, 8534–8537.
4 A. Lennartson, A. Lundin, K. Börjesson, V. Gray and K. Moth-Poulsen, *Dalton Trans.*, 2016, **45**, 8740–8744.
5 J. Orrego-Hernández, A. Dreos and K. Moth-Poulsen, *Acc. Chem. Res.*, 2020, **53**, 1478–1487.
6 K. Jorner, A. Dreos, R. Emanuelsson, O. El Bakouri, I. F. Galván, K. Börjesson, F. Feixas, R. Lindh, B. Zietz, K. Moth-Poulsen and H. Ottosson, *J. Mater. Chem. A*, 2017, **5**, 12369–12378.
7 N. Ree, M. Koerstz, K. V. Mikkelsen and J. H. Jensen, *J. Chem. Phys.*, 2021, **155**, 184105.
8 Z. Refaa, A. Hofmann, M. F. Castro, J. O. Hernandez, Z. Wang, H. Hölzel, J. W. Andreasen, K. Moth-Poulsen and A. S. Kalagasidis, *Appl. Energy*, 2022, **310**, 118541.
9 C. Schøttler, S. K. Vegge, M. Cacciarini and M. B. Nielsen, *ChemPhotoChem*, 2022, **6**, e202200037.
10 M. Brøndsted Nielsen, N. Ree, K. V. Mikkelsen and M. Cacciarini, *Russ. Chem. Rev.*, 2020, **89**, 573–586.
11 A. Vlasceanu, B. N. Frandsen, A. B. Skov, A. S. Hansen, M. G. Rasmussen, H. G. Kjaergaard, K. V. Mikkelsen and M. B. Nielsen, *J. Org. Chem.*, 2017, **82**, 10398–10407.
12 J. Mogensen, O. Christensen, M. D. Kilde, M. Abildgaard, L. Metz, A. Kadziola, M. Jevric, K. V. Mikkelsen and M. B. Nielsen, *Eur. J. Org. Chem.*, 2019, **2019**, 1986–1993.
13 B. Zhang, Y. Feng and W. Feng, *Nano-Micro Lett.*, 2022, **14**, 138.
14 M. A. Gerkman, R. S. L. Gibson, J. Calbo, Y. Shi, M. J. Fuchter and G. G. D. Han, *J. Am. Chem. Soc.*, 2020, **142**, 8688–8695.
15 Y. Shi, M. A. Gerkman, Q. Qiu, S. Zhang and G. G. D. Han, *J. Mater. Chem. A*, 2021, **9**, 9798–9808.

16 Q. Qiu, Y. Shi and G. G. D. Han, *J. Mater. Chem. C*, 2021, **9**, 11444–11463.
17 J. Calbo, C. E. Weston, A. J. P. White, H. S. Rzepa, J. Contreras-García and M. J. Fuchter, *J. Am. Chem. Soc.*, 2017, **139**, 1261–1274.
18 Q. Qiu, S. Yang, M. A. Gerkman, H. Fu, I. Aprahamian and G. G. D. Han, *J. Am. Chem. Soc.*, 2022, **144**, 12627–12631.
19 A. Lennartson, A. Roffey and K. Moth-Poulsen, *Tetrahedron Lett.*, 2015, **56**, 1457–1465.
20 C. L. Sun, C. Wang and R. Boulatov, *ChemPhotoChem*, 2019, **3**, 268–283.
21 D. Bléger and S. Hecht, *Angew. Chem., Int. Ed.*, 2015, **54**, 11338–11349.
22 L. N. Lameijer, S. Budzak, N. A. Simeth, M. J. Hansen, B. L. Feringa, D. Jacquemin and W. Szymanski, *Angew. Chem., Int. Ed.*, 2020, **59**, 21663–21670.
23 L. Stricker, M. Böckmann, T. M. Kirse, N. L. Doltsinis and B. J. Ravoo, *Chem.–Eur. J.*, 2018, **24**, 8639–8647.
24 A. Gonzalez, E. S. Kengmana, M. V. Fonseca and G. G. D. Han, *Mater. Today Adv.*, 2020, **6**, 100058.
25 A. B. Grommet, L. M. Lee and R. Klajn, *Acc. Chem. Res.*, 2020, **53**, 2600–2610.
26 B. L. Diffey, *Methods*, 2002, **28**, 4–13.
27 Y. Yang, R. P. Hughes and I. Aprahamian, *J. Am. Chem. Soc.*, 2012, **134**, 15221–15224.
28 Y. Yang, R. P. Hughes and I. Aprahamian, *J. Am. Chem. Soc.*, 2014, **136**, 13190–13193.
29 Y. P. Wang, Z. X. Zhang, M. Xie, F. Q. Bai, P. X. Wang and H. X. Zhang, *Dyes Pigm.*, 2016, **129**, 100–108.
30 M. Moreno, R. Gelabert and J. M. Lluch, *ChemPhysChem*, 2016, **17**, 2824–2838.
31 H. Qian, Y. Y. Wang, D. S. Guo and I. Aprahamian, *J. Am. Chem. Soc.*, 2017, **139**, 1037–1040.
32 X. Huang, Z. Shangguan, Z. Y. Zhang, C. Yu, Y. He, D. Fang, W. Sun, Y. C. Li, C. Yuan, S. Wu and T. Li, *Chem. Mater.*, 2022, **34**, 2636–2644.
33 Z. Y. Zhang, Y. He, Z. Wang, J. Xu, M. Xie, P. Tao, D. Ji, K. Moth-Poulsen and T. Li, *J. Am. Chem. Soc.*, 2020, **142**, 12256–12264.
34 Y. Yang, S. Huang, Y. Ma, J. Yi, Y. Jiang, X. Chang and Q. Li, *ACS Appl. Mater. Interfaces*, 2022, **14**, 35623–35634.
35 P. J. Flory and A. Vrij, *J. Am. Chem. Soc.*, 1963, **85**, 3548–3553.
36 M. G. Broadhurst, *J. Chem. Phys.*, 1962, **36**, 2578–2582.
37 W. Sun, Z. Shangguan, X. Zhang, T. Dang, Z.-Y. Zhang and T. Li, *ChemSusChem*, 2023, e202300582.
38 L. Kortekaas, J. Simke, D. W. Kurka and B. J. Ravoo, *ACS Appl. Mater. Interfaces*, 2020, **12**, 32054–32060.
39 E. Madiahlagan, B. N. Sunil, Z. Ngaini and G. Hegde, *J. Mol. Liq.*, 2019, **292**, 111328.
40 Z. Wang, R. Losantos, D. Sampedro, M. A. Morikawa, K. Börjesson, N. Kimizuka and K. Moth-Poulsen, *J. Mater. Chem. A*, 2019, **7**, 15042–15047.
41 J. Olmsted, J. Lawrence and G. G. Yee, *Sol. Energy*, 1983, **30**, 271–274.
42 D. E. Williams, C. R. Martin, E. A. Dolgopolova, A. Swifton, D. C. Godfrey, O. A. Ejegbavwo, P. J. Pellechia, M. D. Smith and N. B. Shustova, *J. Am. Chem. Soc.*, 2018, **140**, 7611–7622.
43 A. H. Heindl, R. C. Wende and H. A. Wegner, *Beilstein J. Org. Chem.*, 2018, **14**, 1238–1247.
44 C. Di Berardino, M. A. Strauss, D. Schatz and H. A. Wegner, *Chem.–Eur. J.*, 2022, **28**, 128.
45 L. Schweighauser, M. A. Strauss, S. Bellotto and H. A. Wegner, *Angew. Chem., Int. Ed.*, 2015, **54**, 13436–13439.
46 A. Kunz, A. H. Heindl, A. Dreos, Z. Wang, K. Moth-Poulsen, J. Becker and H. A. Wegner, *ChemPlusChem*, 2019, **84**, 1145–1148.
47 J. Volkmann, D. Kohrs and H. A. Wegner, *Chem.–Eur. J.*, 2023, **29**, e202300268.
48 C. Özçoban, T. Halbritter, S. Steinwand, L. M. Herzig, J. Kohl-Landgraf, N. Askari, F. Groher, B. Fürtig, C. Richter, H. Schwalbe, B. Suess, J. Wachtveitl and A. Heckel, *Org. Lett.*, 2015, **17**, 1517–1520.
49 C. Petermayer, S. Thumser, F. Kink, P. Mayer and H. Dube, *J. Am. Chem. Soc.*, 2017, **139**, 15060–15067.
50 M. Clerc, F. Stricker, S. Ulrich, M. Sroda, N. Bruns, L. F. Boesel and J. Read de Alaniz, *Angew. Chem., Int. Ed.*, 2021, **60**, 10219–10227.
51 J. R. Hemmer, Z. A. Page, K. D. Clark, F. Stricker, N. D. Dolinski, C. J. Hawker and J. Read De Alaniz, *J. Am. Chem. Soc.*, 2018, **140**, 10425–10429.